Energy 255 (2022) 124437

Contents lists available at ScienceDirect

Energy

journal homepage: www.elsevier.com/locate/energy

HMF hydrogenolysis over carbon-supported Ni–Cu catalysts to produce hydrogenated biofuels

Nerea Viar [a, *], Jesus M. Requies [a], Ion Agirre [a], Aitziber Iriondo [a], Cristina García-Sancho [b], Pedro L. Arias [a]

[a] Chemical and Environmental Engineering Department. Engineering Faculty of Bilbao, University of Basque Country (UPV/EHU), Plaza Ingeniero Torres Quevedo 1 – 48013, Bilbao, Spain
[b] Universidad de Málaga, Departamento de Química Inorgánica, Cristalografía y Mineralogía (Unidad Asociada al ICP-CSIC), Facultad de Ciencias, Campus de Teatinos, 29071 Málaga, Spain

ARTICLE INFO

Article history:
Received 13 January 2022
Received in revised form
13 May 2022
Accepted 30 May 2022
Available online 2 June 2022

Keywords:
Bimetallic catalyst
Ni–Cu
DMF
DMTHF
Hydrogenolysis
Biomass-derived carbon

ABSTRACT

Non-noble monometallic and bimetallic catalysts supported in biomass-derived carbon were tested in the 2,5-dimethylfuran (DMF) and 2,5-dimethyltetrahydrofuran (DMTHF) production from 5-hydroxymethylfurfural (HMF) hydrogenolysis using a fixed-bed continuous-flow reactor. These support and reaction system were selected in order to obtain a more sustainable catalyst development and to implement a continuous flow reaction system. The carbon-supported biomass-derived catalysts were compared with catalysts supported on commercial carbons, which were treated with acid to remove impurities. All the bimetallic catalysts exhibited high stability after 25 h-on stream, achieving DMF yields above 50% and complete HMF conversion. Biomass-derived carbon supported catalysts seems more selective toward DMF during the 8-9 h-on stream than commercial carbon supported ones. The good activity and stability of the bimetallic catalysts seems to be related to the synergistic effect between acid and metallic sites, exhibiting the most promising ones an excellent stability for 46 h on stream. Monometallic catalysts exhibited high yields, above 70%, at the beginning of the reaction. However, they suffer from partial deactivation, probably due to metal sintering. Finally, the obtained catalytic activities and selectivities toward target products are close to the reported ones for discontinuous systems, being an important aspect for its possible industrial application.

1. Introduction

The need to limit the increase in global temperature and the growth in world energy demand, both of which are related to the rise in CO_2 emissions, call for a significant transformation in the energy supply [1]. The transportation sector accounted for 30% increase in energy consumption in the last decade [2]. Conventional fuels, derived from oil refining, are the predominant energy source for transportation [3].

Lignocellulosic biomass-derived products are excellent candidates for replacing conventional gasoline. This green feedstock is the only renewable resource that can substitute oil-derived chemicals and fuels [4]. They are composed of cellulose, hemicellulose, and lignin. Cellulose is the main component (40–50%) and can be hydrolyzed into glucose. This C_6 molecule can be further dehydrated into 5-hydroxymethylfurfural (HMF), a platform molecule in Bozell and Petersen's "Top 10 + 4" list [5], which includes the most interesting and promising biorefinery compounds.

HMF contains an aldehyde group (–C=O) and a hydroxyl group (–OH) attached to a furan ring. These functional groups can be selectively reduced to 2,5-dimethylfuran (DMF) and 2,5-dimethyltetrahydrofuran (DMTHF), respectively. Both are suitable biofuel candidates and are promising additives for conventional gasoline [6]. They exhibit similar properties to those of gasoline, which have been summarized in Table 1.

In the last few decades, DMF production using noble and non-noble metal catalysts has been widely studied in batch reaction systems. Ru- [8,9] and Pt-based [10] catalysts have been extensively investigated by varying the operating conditions, solvents, and

* Corresponding author.
E-mail address: nerea.viar@ehu.eus (N. Viar).

https://doi.org/10.1016/j.energy.2022.124437

Table 1
Properties of conventional gasoline and different biofuels [7].

	Conventional gasoline	DMF	DMTHF
Lower heating value ($MJ \cdot kg^{-1}$)	42.7	33.7	38.3
Research Octane number (RON)	90–99	119	82
Boiling point (C)	25–215	92–94	90–92
Density at 20 C ($g \cdot cm^{-3}$)	0.745	0.89	0.83
Viscosity at 40 C ($mm^2 \cdot s^{-1}$)	0.4–0.8	0.65	0.47

reaction time; complete HMF conversion and maximum DMF yield of 70–90% have been achieved. Considering the limited availability and high cost of these noble metals, their commercial application is impractical. Recently, Guo et al. [11] studied the synergistic effect of acid and metal sites on a Ni/ZSM-5 catalyst; excellent DMF production (86.5%) was obtained.

Monometallic Cu catalysts have also been investigated [12–14] using different supports, H_2 donors, and solvents. Finally, the use of bimetallic catalysts based on noble metals [15,16] and non-noble metals [17,18] has been reported. Luo et al. [19] employed Pt–M/C catalysts (M = Ni, Zr, or Cu) for HMF hydrodeoxygenation in a continuous liquid-phase flow reactor; the bimetallic catalysts had higher DMF selectivity values than their corresponding monometallic catalysts. They achieved the highest DMF yield (98%) in the presence of bimetallic Pt–Ni on a carbon catalyst at 200 °C and 33 bar. In general, bimetallic Ni-based catalysts can be employed in a wide range of reactions owing to their tunable chemical/physical properties [20]. Concomitantly, Yang et al. [21] employed Ni–Co/C catalysts for HMF-to-DMF hydrogenolysis in both batch and fixed-bed reactor tests, and the Ni species increased the stability of the CoO_x species. Bimetallic Cu–Co catalysts have also been studied for use in DMF production. Additionally, Guo et al. [22] synthesized a bimetallic Cu–Co catalyst supported on N-graphene-modified Al_2O_3 for HMF hydrogenolysis. The catalyst resulted in high DMF yields (>99%) because it activated C–O bond cleavage and C=O bond hydrogenation. However, the catalyst could not hydrogenate the C=C bond in the furan ring without yielding 2,5-bis(hydroxymethyl)tetrahydrofuran and DMTHF. Srivastava et al. [23] studied the influence of different supports (CeO_2, ZrO_2, and Al_2O_3) of Cu–Co-based catalysts on DMF production; the Cu–Co/Al_2O_3 catalyst had the highest DMF selectivity. Chen et al. [24] also observed a synergistic effect between Cu and Co using carbon-coated Cu–Co bimetallic nanoparticles as catalysts for DMF production. They confirmed that the bimetallic nanoparticles were entrapped by the carbon shells, which prevented the oxidation and deactivation of the catalysts. Similarly, Sarkar et al. [25] synthesized Cu–Pd bimetallic nanoparticles embedded in a carbon matrix by pyrolyzing metal–organic frameworks; the catalyst stability was enhanced. Because Cu and Ni were demonstrated to activate DMF production, Gupta et al. [26] supported both the metals on hydrotalcite (HT) for the catalytic hydrogenation of HMF. DMF and DMTHF yields of 67% and 32%, respectively, were achieved after 15 h under 10 bar of H_2 at 90 °C in batch conditions.

In addition, the production of DMTHF from HMF has attracted attention. Gao et al. [27] synthesized a N-doped decorated Cu-based catalyst (NC–Cu/MgAlO) using cyclohexanol as the hydrogen donor and solvent and observed high DMTHF yields. Similarly, Chen et al. [28] reported that the HMF-to-DMF conversion was rapid, but the hydrogenation of the furan ring was slow, when a Ni/SBA-15 catalyst was used.

Most abovementioned investigations are focused on the production of DMF or DMTHF in batch systems. However, at an industrial scale, continuous processes lead to higher efficiencies and lower production costs than batches. Therefore, highly efficient catalytic systems must be explored and tested under continuous operation. In this study, non-noble-metal-based Ni–Cu bimetallic catalysts were synthesized using various supports. Their activities and stabilities were investigated in a gas-phase continuous fixed-bed reactor. Biomass-derived carbon was employed as the catalyst support because of its great potential as a sustainable material in different industrial sectors; moreover, it does not produce any waste (net zero waste) and facilitates the development of a circular economy [29]. Biomass-derived carbons exhibit excellent textural and chemical properties, such as large specific surface area, high porosity, and abundant surface functionalities [30]. Furthermore, bimetallic Ni-based catalysts can be employed in a wide range of reactions owing to their tunable chemical/physical properties [31].

This study aims to synthesize two value-added products—DMF and DMTHF—from HMF hydrogenolysis in the most sustainable and efficient way possible. To achieve this, continuous systems such as fixed-bed reactors were tested herein. Although most studies have employed discontinuous batch reactors, continuous processes lead to high efficiencies and low production costs at the industrial scale. Previous studies have proven that Ni–Cu bimetallic catalysts have good characteristics in HMF hydrogenolysis in fixed-bed reactors [33]. The present study proceeds one step further and attempts to develop a highly sustainable catalyst using a carbonaceous derivative of local waste biomass and incorporating Ni and Cu (active metals) as supports. Further, stability and reusability tests have been performed with the most promising bimetallic catalyst.

2. Experimental

2.1. Reaction system

Activity tests were conducted in a bench-scale fixed-bed reactor in which 500 mg catalyst was diluted with inert CSi (1:9 wt). Synthetic HMF (Sigma-Aldrich, 99%) diluted in 1-butanol (1.5 wt %) was fed (WHSV of 0.15 h^{-1} ($g_{HMF} \cdot g_{cat}^{-1} \cdot h^{-1}$)) into the aforementioned reaction system using a high-performance liquid chromatography (HPLC) pump, once 275 °C and 15 bar of pure H_2 were reached. Under these operating conditions, the HMF hydrogenolysis reaction was performed in the gas phase in accordance with thermodynamic calculations as well as data published in the open literature [32]. Moreover, no pre-reduction step was required for the catalyst because the catalyst was reduced under the operating conditions. A previous study [7] demonstrated that the activity results did not differ on the basis of pre-reduced or non-pre-reduced catalyst, inferring the successful activation of the catalyst under the operating conditions prior to starting the reaction.

The HMF conversion and DMF and DMTHF yield values were used to describe the activity results (see Equations (1) and (2), where N is the molar flowrate in $mol \cdot min^{-1}$).

$$\text{HMF conversion } (\%) = \frac{N_{HMF}^{in} - N_{HMF}^{out}}{N_{HMF}^{in}} \cdot 100 \quad (1)$$

$$\text{DMF and DMTHF yield } (\%) = \frac{N_{DMF/DMTHF}^{out}}{N_{HMF}^{in}} \cdot 100 \quad (2)$$

2.2. Analysis

The condensed liquid products were analyzed by HPLC (HPLC 1260 Infinity equipped with a Hi-Plex H column and an infrared detector) to quantify HMF conversion and by gas chromatography (Agilent 6804 GC equipped with a SupraWax 280 capillary column

and a flame ionization detector) to quantify DMF and DMTHF yields. Other possible byproducts—2,5-bis(hydroxymethyl)furan (BHMF), 5-methylfurfural (5-MF), and 5-methylfurfuryl alcohol (MFA)—were also analyzed by gas chromatography. The error of the reaction system and the analysis was ±5%.

2.3. Catalyst preparation

Various catalytic supports were prepared. Two different carbons were employed in this study, namely, commercial carbon (PanReac, granulated n° 2) and biomass-derived carbon provided by Envirohemp S.L, an activated carbon produced from local waste biomass that was activated by chemical activation (acidic route). Both the carbons were modified with kaolin (Merck) to obtain the desired mechanical resistance [33]. For the modification, 40 wt % kaolin (K) and the prepared supports were mixed with deionized water in a rotatory evaporator. After stirring the mixture for 2 h, it was heated to 80 °C, and water was evaporated under vacuum. After drying the supports overnight, they were thermally treated at 500 °C for 2 h under an inert N_2 atmosphere. The obtained supports (carbon + kaolin) were designated *commercial carbon (CC)* and *biomass-derived carbon (BC)*. Some authors have reported the requirement of a purification process—treatment with nitric acid to remove inorganic impurities [34] and/or undesirable ash [35]. To determine whether the purification process affects the activity, the aforementioned modified supports (commercial carbon and biomass-derived carbon) were further treated with an acid solution. The supports were stirred in a solution of 10% (v/v) HNO_3 at 80 °C for 2 h at 200 rpm [36]. Subsequently, they were washed with distilled water, neutralized with 0.1 M of NaOH to achieve a pH of 7, and placed in an oven at 180 °C for 6 h to remove the volatile matter. These supports were labeled *treated commercial carbon (TCC)* and *treated biomass-derived carbon (TBC)*.

On the one hand, only carbon + kaolin supports (with or without acidic purification) were used to synthesize the catalysts. However, bare carbons (without kaolin) were also characterized to analyze the differences. For catalyst synthesis, $Cu(NO_3)_2 \cdot H_2O$ (Alfa Aesar, 98%) and $Ni(NO_3)_2 \cdot 6H_2O$ (Sigma-Aldrich, 99.99%) were employed as active-metal phase precursors.

For the monometallic catalysts, 15 wt % Ni or Cu was impregnated in CC and BC by wetness impregnation. After drying overnight, thermal treatment was performed under N_2 at 500 °C for 2 h. The catalysts were designated *Ni/CC*, *Ni/BC*, *Cu/CC*, and *Cu/BC*.

Bimetallic catalysts were synthesized in sequential steps. First, 15 wt % Cu was loaded in the kaolin-modified CC and BC supports by wetness impregnation. Then, the Cu-loaded carbon supports were dried overnight and thermally treated at 500 °C for 2 h under a N_2 atmosphere. Finally, 15 wt % Ni was impregnated using the same method. The preparation method of the bimetallic catalyst was optimized in previous investigations [37]. The obtained catalysts were labeled *Ni–Cu/CC* and *Ni–Cu/BC*.

On the other hand, only TCC and TBC supports were used for the bimetallic-catalyst synthesis owing to the stability issues while testing the monometallic catalysts. The procedure for synthesizing these treated-carbon-impregnated bimetallic catalysts was identical to that described previously. The obtained catalysts were labeled *Ni–Cu/TCC* and *Ni–Cu/TBC*.

2.4. Catalyst characterization

2.4.1. Elemental analysis (CHN)

Elemental analysis of bare carbons (before the addition of kaolin) was performed to understand the differences in the composition of CC and BC. The effect of acidic treatment on the elemental composition was also examined.

The samples were placed in a vertical quartz reactor and heated at 980 °C under a constant flow of He stream. A few seconds after introducing the sample, the He stream was enriched with high-purity O_2. The combustion gas mixture was driven through a tungsten oxide zone to achieve complete quantitative oxidation, followed by a reduction step in a Cu zone to reduce nitrogen oxides to nitrogen. The resulting components, namely, N_2, CO_2, and H_2O, were separated using a chromatographic column and detected using a thermal conductivity detector (TCD). The analysis method follows ISO 17025 and the uncertainty values are ±6% for C, ± 10% for H and ±3% for N, which were quantified by means of black box modelling.

2.4.2. Inductively coupled plasma optical emission spectroscopy (ICP-OES)

The thermally treated catalysts were dissolved in an acid solution (25% HNO_3 and 75% HCl) in a Milestone microwave digestion system ETHOS 1, and the obtained solution was analyzed by ICP-OES (PerkinElmer Optima 3300DV) to measure the metal content. The error in the measurements was ±3%.

2.4.3. Textural properties

The thermally treated samples were outgassed at 150 °C for 4 h, and N_2 adsorption–desorption isotherms were then acquired at −198 °C using Autosorb1C/TCD (Quantachrome, USA) to calculate the surface area using the BET equation. The micropore area was not analyzed herein (using the Dubinin–Raduskevich equation) because Ni and Cu were incorporated on the outer support surface or on the mesopores. The pore volume and average pore diameter were calculated using the Barrett–Joyner–Halenda (BJH) method. The error in the measurements was ±5%,

2.4.4. Temperature-programmed desorption with ammonia (NH_3-TPD)

The thermally treated samples were reduced *in situ* at 275 °C for 1 h, and the physisorbed impurities were desorbed by a He stream for 30 min. After cooling the sample to 100 °C, NH_3 was flowed over the sample. The physisorbed NH_3 was eliminated by increasing the temperature to 150 °C. Finally, the samples were heated to 850 °C, and the desorbed NH_3 was detected using a TCD detector. The error in the measurements was ±5%,

2.4.5. X-ray diffraction (XRD)

The X-ray diffraction patterns of the freshly reduced and used catalysts were obtained using Seifert XRD 3000 diffractometer equipped with a PW 2200 Bragg-Brentano u/2u goniometer, a bent graphite monochromator, and an automatic slit, using Cu K radiation (0.15418 nm) and 0.028° step size for scanning. The crystallite sizes of the observed peaks were calculated using the Scherrer equation. The error in the measurement was ±10%.

2.4.6. Transmission electron microscopy (TEM)

The TEM images were acquired using FEI Talos F200X equipment (Thermo Fisher Scientific) to study the morphology of peculiar freshly reduced and used catalysts. This equipment combines high-resolution STEM and TEM imaging with energy dispersive X-ray spectroscopy (EDS) signal detection, that is, 3D chemical characterization with compositional mapping. To analyze the samples, they were dispersed in ethanol, and a drop of the suspension was placed on a Cu grid (300 mesh). The error in the measurements was ±7%.

The metallic dispersion was calculated from the size measurement of 200 particles in accordance with the method described by Borodziński and Bonarowska [38]. In this procedure, the atomic ratio of the particles is required for the calculation. For the

monometallic catalysts, the atomic ratios of metallic Ni and Cu were employed. In the case of bimetallic catalysts, the atomic ratio was calculated on the basis of a previously reported assumption [39]—the contribution of each metal to the atomic ratio is associated with the metallic contents of Ni and Cu obtained by ICP-OES.

2.4.7. X-ray photoelectron spectroscopy (XPS)

The surface elemental compositions and oxidation states of the freshly reduced and used catalysts were analyzed by XPS. The samples were analyzed using a VG Escalab 200R spectrometer equipped with a hemispherical electron analyzer and an Al K1 (h = 1486.6 eV) 120 W X-ray source. A stainless steel sample holder was used to deposit the samples. First, the samples were degassed at 300 °C in a pretreatment chamber. The base pressure of the spectrometer is typically 910 Torr (0.0133 bar). The spectra were collected at a pass energy of 20 eV, which is usually considered a high-resolution condition. The error in the measurements was ±5%.

3. Results and discussion

3.1. Catalyst characterization results

The characterization results obtained using different techniques are described in this section. The supports were first thermally treated under an inert N_2 atmosphere at 500 °C for 2 h for evaluation under the same conditions as those of the synthesized catalysts.

The XRD, TEM, and XPS characterization techniques do not facilitate the *in situ* reduction process. Thus, the fresh catalysts were reduced ex situ in a horizontal oven at 275 °C for 2 h under pure H_2 gas flow. The samples were then stored in isooctane to avoid possible oxidation under atmospheric conditions. This storage procedure was employed for the catalysts as well.

3.1.1. Elemental analysis (CHN)

The elemental compositions of the bare carbonaceous materials, as obtained from the CHN analyses, are summarized in Table 2. The percentage of oxygen was determined by the difference.

Commercial carbon and biomass-derived carbon supports have similar compositions but different hydrogen contents. In contrast, the treated commercial carbon and biomass-derived carbon supports have a higher oxygen content than the untreated supports. The acid treatment of the commercial carbon and biomass-derived carbon supports with HNO_3 apparently favors the oxidation of the carbonaceous materials [40,41] owing to the oxidizing capacity of HNO_3.

3.1.2. Chemical and textural properties

The textural properties, as determined using the N_2-physisorption technique, of different supports (bare supports and kaolin-modified supports) and catalysts are summarized in Table 3 and Table 4, respectively.

The CC and BC materials have high, comparable BET surface areas (>970 $m^2\ g^{-1}$). However, BC exhibits higher pore volume and pore diameter than CC. In both materials, the acidic treatment slightly alters the textural properties, resulting in low BET surface area and significantly high average pore diameter of the treated carbons. According to the literature [32] the strong oxidation due to acid treatment can decrease the BET surface area and microporous structure. Finally, the addition of kaolin reduces the total surface area, as inferred from the low surface area of bare kaolin (18 $m^2\ g^{-1}$). Additionally, kaolin addition affects the porosity of the supports owing to the blockage of different types of pores.

The monometallic catalysts have lower specific surface areas (240–310 $m^2\ g^{-1}$) than the supports (Table 4), most probably owing to the partial blockage of the pores of the support by metal deposition [42]. This effect is profound in the case of the bimetallic catalyst (120–190 $m^2 g^{-1}$), which is associated with the high metal loadings of these catalysts and large obstruction of the porous structure. This phenomenon has also been observed by Andrade et al. [43]. This effect signifies that the metals are deposited not on the micropore structure but possibly deposited on the support surface and on the mesopores, in the case of the biomass-derived carbon. In general, catalysts supported on BC have low BET surface areas, which is probably associated with different pore size distributions. This trend is much profound for the monometallic catalysts.

The real metal contents of the catalysts, studied by ICP-OES (Table 4), are similar to the nominal values, except for the bimetallic catalysts supported on carbons without acid pretreatment. The high carbon concentrations and high specific surface areas of these supports, as determined by CHN analysis and N_2-physisorption, respectively, apparently favor metal deposition. However, a more plausible explanation would be that the two thermal treatments of the catalysts after incorporating Cu and then Ni could cause partial thermal decomposition of the carbon, resulting in higher metal loadings than the nominal ones.

3.1.3. Temperature programmed desorption with ammonia (NH_3-TPD)

The surface acidity of the bare supports (CC, BC, TCC, and TBC) and the prepared catalysts was investigated by NH_3-TPD. The results are shown in Fig. 1.

The CC support has a lower acidity than the BC support. Moreover, the addition of kaolin significantly decreases the acidity of the BC support [33], possibly because bare kaolin has a low acidity (Fig. 1) and its incorporation blocks the acid sites. As mentioned above, the data in Table 3 indicates the incorporation of kaolin into the surface and porous structure of the BC support, resulting in low specific surface area, pore volume, and average pore diameter. Moreover, acid pretreatment decreases the acidity of both the CC and BC supports. Further, despite the significant difference in the acidities of pure commercial carbon (0.64 mmol $NH_3 \cdot g_{cat}^{-1}$) and biomass-derived carbon (1.42 mmol $NH_3 \cdot g_{cat}^{-1}$) (Fig. 1), both carbons have nearly identical acidities (0.62 and 0.64, respectively) after modification with kaolin. A similar effect is observed for the acid-pretreated carbons, in which the addition of kaolin results in similar acidities of approximately 0.44 mmol $NH_3 \cdot g_{cat}^{-1}$.

The incorporation of Ni into the K-modified supports enhances the acidity of the monometallic catalysts. Moreover, nonreduced Ni^{2+} species act as Lewis acid sites, thereby increasing the total acidity of the catalyst [44,45]. The high acidity of the catalyst supported on BC agrees well with the XPS results (explained below in Section 3.1.6), in which the catalyst surface has high Ni^{2+} content because of increase in the acidity. In contrast, monometallic Cu catalysts have lower acidities than the supports. Cu particles could either be covered by or have reacted with the acidic sites, reducing the total acidity of the catalysts [43].

The bimetallic catalyst and the supports have similar acidities.

Table 2
Elemental analysis of carbon supports determined by CHN analyses.

Bare carbons	C (%)	H (%)	N (%)	O[b] (%)
Commercial carbon[a]	80.29	0.85	0.61	18.25
Treated commercial carbon[a]	69.83	2.00	0.98	27.19
Biomass-derived carbon[a]	77.67	2.61	0.38	19.34
Treated biomass-derived carbon[a]	67.76	1.41	0.94	29.89

[a] Bare carbons (without kaolin).
[b] Calculated by difference.

Table 3
Textural properties of thermally treated supports (obtained from N_2-physisorption).

Supports	BET ($m^2 \cdot g^{-1}$)	Pore volume ($cm^3 \cdot g^{-1}$)	Average pore diameter (nm)
Commercial carbon	991	0.05	1.8
Commercial carbon (with kaolin)	767	0.01	1.9
Treated commercial carbon	964	0.04	2.2
Treated commercial carbon (with kaolin)	744	0.09	2.4
Biomass-derived carbon	977	0.47	3.5
Biomass-derived carbon (with kaolin)	715	0.11	2.5
Treated biomass-derived carbon	912	0.47	3.6
Treated biomass-derived carbon (with kaolin)	482	0.29	4.0
Kaolin	18	0.09	21.6

Table 4
Chemical and textural properties of different catalysts.

Catalysts	BET[a] ($m^2 \cdot g^{-1}$)	Pore volume[a] ($cm^3 \cdot g^{-1}$)	Average pore diameter[a] (nm)	Cu[b] (%)	Ni[b] (%)
Ni/CC	309	0.09	3.1	–	15
Ni/BC	241	0.12	3.6	–	16
Cu/CC	282	0.06	2.7	15	–
Cu/BC	311	0.19	4.1	15	–
Ni–Cu/CC	143	0.05	3.3	21	23
Ni–Cu/TCC	190	0.04	2.8	16	16
Ni–Cu/BC	135	0.08	3.8	22	22
Ni–Cu/TBC	119	0.05	3.4	14	17

Obtained from [a]N_2-physisorption and [b]ICP-OES.

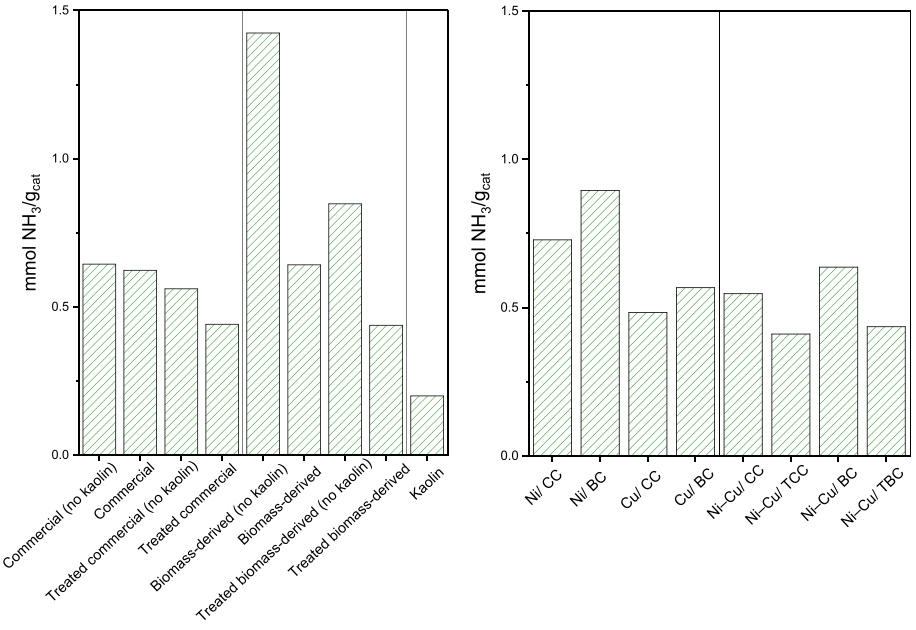

Fig. 1. Amount of NH_3 desorbed from different thermally treated supports and catalysts, as determined by NH_3-TPD.

Presumably, even if some acidic sites are covered by metallic species, the presence of Ni cations implies the existence of Lewis acid sites, which could compensate for the possible loss of acid sites in the original support [46,47].

3.1.4. X-ray diffraction (XRD)

The X-ray diffraction patterns of the freshly reduced and used catalysts are shown in Fig. S1. The average crystallite sizes of the metallic phases, calculated using the Scherrer equation, are summarized in Table 5. Further, Fig. 2 presents the enlarged graphs of the bimetallic-catalyst profiles.

All the monometallic catalysts present diffraction angles of 35.6°, 41.1°, 60.1°, 71.8°, and 75.6°, which are associated with CSi (used to prepare the catalytic fixed bed to avoid temperature gradients) [48]; the peaks are not shown in Fig. S1. The diffraction patterns of monometallic Ni catalysts (see graphic b in Fig. S1) show diffraction peaks at $2\Theta = 44.5°$, 51.8°, and 76.4°, ascribed to metallic Ni phases [49]. Diffraction angles corresponding to the NiO species ($2\Theta = 37.2°$, 43.3°, 62.9°, and 75.6°) are not observed. These results indicate that most Ni species are in a reduced state [50]. Similarly, Cu-based catalysts exhibit diffraction peaks at $2\Theta = 43.3°$, 50.4°, and 74.1°, attributed to metallic Cu phases [49]. The freshly reduced Cu catalysts also present a peak at approximately 36.4°, which can be ascribed to the Cu_2O species [51]. Moreover, the Cu/CC catalyst exhibits a lower crystallite size than the Cu/BC catalyst, implying better dispersion of Cu species on this support. Ni–based

Table 5
Crystallite size (nm) of different catalysts (operating conditions for used catalysts: T = 275 °C, P_{H_2} = 15 bar, WHSV = 0.15 h^{-1}, and 25 h on stream).

Catalysts	Freshly reduced		Used	
	Ni	Cu	Ni	Cu
Ni/CC	20	–	20	–
Ni/BC	15	–	10	–
Cu/CC	–	40	–	35
Cu/BC	–	45	–	45
Ni–Cu/CC	10[a]		15[a]	
Ni–Cu/TCC	10	30	10	35
Ni–Cu/BC	15[a]		5 (NiO)	15 (CuO)
Ni–Cu/TBC	15	20	15	25

[a] Ni–Cu crystallites.

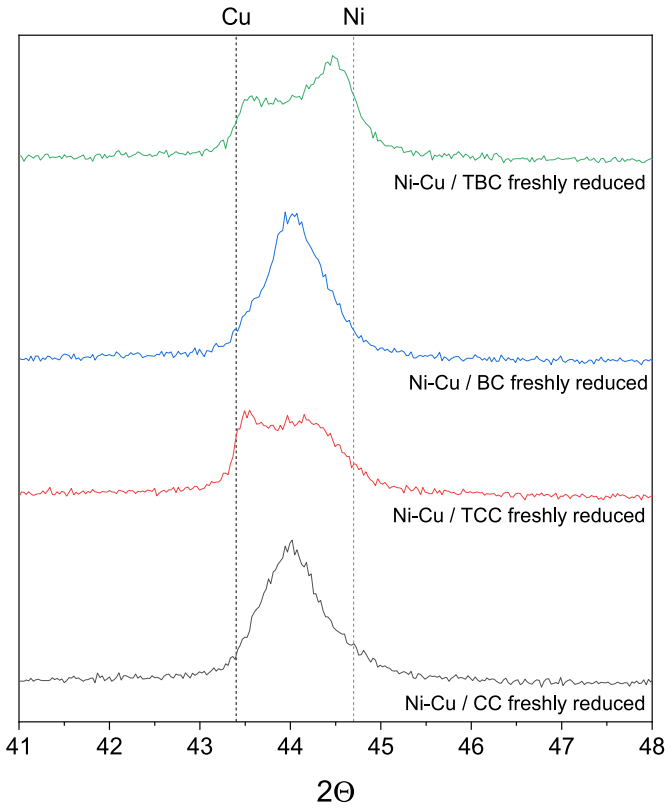

Fig. 2. X-ray diffraction patterns of freshly reduced bimetallic catalysts (enlarged graph).

monometallic catalysts present a lower crystallite size than Cu-based catalysts [52]. After the reaction, all monometallic catalysts exhibit crystallite sizes similar to those of the initial ones, revealing the good stability of the metallic phases in these catalysts during the reaction.

The bimetallic catalysts exhibit several Ni and Cu diffraction peaks, as shown in Fig. 2, indicating possible interactions between the Ni and Cu species. The freshly reduced catalysts supported on CC and BC exhibit characteristic and well-defined diffraction peaks related to a Cu–Ni alloy phase ($2\theta = 43.7°$ and $50.9°$). This alloy has small crystallites with a size of 10–15 nm. The diffraction profiles of the bimetallic catalysts supported on TCC and TBC reveal two peaks at approximately 43.7° and 50.9°. The first and second peaks can be attributed to Cu-rich and Ni-rich alloys, respectively. Among these samples, the Cu-rich alloy has a larger crystallite (20–30 nm), which increases during the reaction, possibly owing to sintering. In contrast, the Ni-rich alloy has stable crystallites sized 10–15 nm. The existence of two different Ni–Cu alloys in the catalyst has been reported previously [43,53]. Moreover, even though there are two peaks, they are located at an intermediate position, implying the formation of Ni–Cu alloy and not that of pure Ni and pure Cu crystals.

3.1.5. Transmission electron microscopy (TEM)

The morphology, size, and dispersion of the metallic particles of peculiar catalysts were investigated by TEM. The dispersion and mean particle size were calculated in accordance with the procedure described by Borodziński and Bonarowska [38] and the calculation results are summarized in Table 6. Select images of the freshly reduced and used catalyst are presented in Fig. S2. Further, the corresponding histograms and profiles of the accumulated frequencies are shown in Fig. S3. Additionally, select elemental-mapping images, which reveal the distribution of elements within the catalysts, are shown in Fig. 3.

As shown in Table 6 and Figs. S2 and S3, the freshly reduced samples of monometallic Ni and Cu catalysts exhibit similar dispersions and particle sizes. However, the particle size increases during the reaction, which decreases the total dispersion of the catalysts. The increase in size can be related to the sintering of metallic particles. This effect is comparatively more evident for the Cu/CC catalyst.

In the case of the bimetallic catalysts, the dispersions and particle sizes of the freshly reduced catalysts supported on CC and BC are significantly different. Apparently, CC disperses the particles more efficiently than BC, increasing the active metal exposure on the surface. This observation is in agreement with the S_{BET} results. The CC support has a higher BET surface area than the BC support, providing a better dispersion of metallic species. Another hypothesis deals with the acidity of the carbon surface created during activation. However, the metal particles grow during the reaction in the case of the bimetallic catalyst, especially for the Ni–Cu/CC catalyst, implying a reduction in the total dispersion of the catalyst. This phenomenon is also confirmed by the XRD data.

The elemental mapping demonstrates that monometallic catalysts contain only Ni and Cu species, whereas the bimetallic catalysts mainly contain a combination of Ni and Cu species associated with the Ni–Cu alloy, as detected by XRD.

3.1.6. X-ray photoelectron spectroscopy (XPS)

The surface elemental composition (Fig. 4) and oxidation state (Fig. 5) of the freshly reduced and used catalysts were examined by XPS. The Ni 2*p*, Cu 2*p*, and Cu LMM deconvoluted profiles of peculiar catalysts are included in the Supporting Information (Figs. S4 and S5). The carbon content increases in all the used catalysts, probably because of coke deposition on the surface during the reaction, which implies deactivation of the catalysts.

The surface metal content of the monometallic catalysts is high

Table 6
Dispersion and metallic particle size of peculiar freshly reduced and used catalysts (operating conditions: T = 275 °C, P_{H_2} = 15 bar, WHSV = 0.15 h^{-1}, and 25 h on stream).

Catalysts	State	d_{mean} (nm)	Dispersion (%)
Ni/CC	Freshly reduced	23	5
	Used	32	4
Cu/CC	Freshly reduced	26	5
	Used	42	3
Ni–Cu/CC	Freshly reduced	12	11
	Used	27	5
Ni–Cu/BC	Freshly reduced	30	4
	Used	36	3

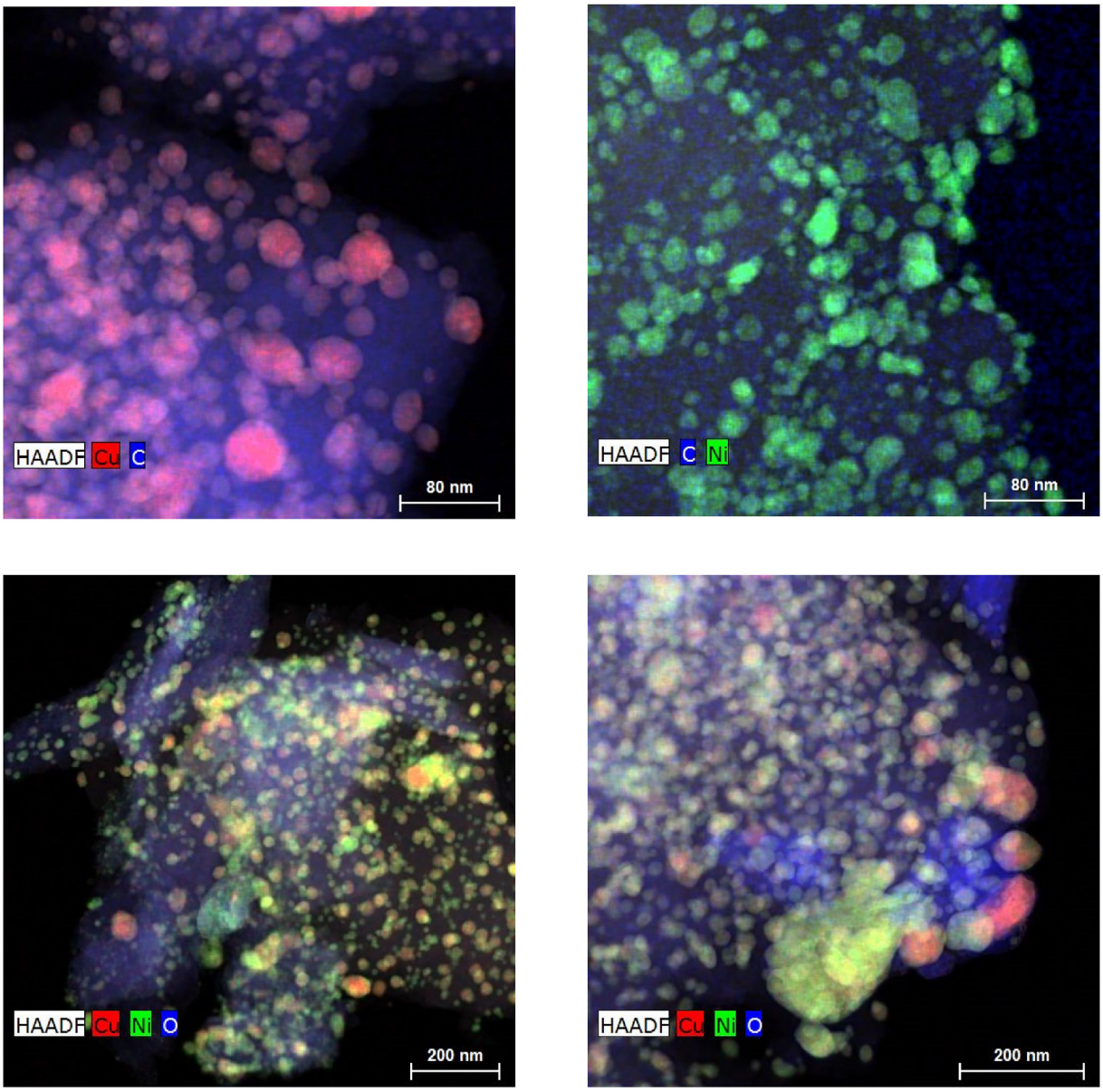

Fig. 3. TEM images with the corresponding elemental mapping of the freshly reduced catalysts: a) Cu/CC, b) Ni/CC, c) Ni–Cu/CC d) Ni–Cu/BC.

in the case of CC support. The higher BET surface area, observed using the N_2 physisorption technique, and the higher C content in the support, detected by CHN analysis, can favor more deposition of the active-metal phase on the catalyst surface. However, the metal content decreases after the reaction for these catalysts, possibly as a result of coke deposition on the metallic sites or sintering, as observed by XRD and TEM.

The bimetallic catalyst supported on the TBC has low surface metal content, probably resulting from a decrease in the metallic particle dispersion. As inferred by the textural property data, this particularity can be related to the lower BET surface area presented by the TBC support than that by the CC, BC, and TCC supports. After the reaction, the metal content of the bimetallic catalysts decreases, presumably because of coke deposition or sintering. The Ni/Cu ratio is higher than the bulk ratio obtained from the - ICP-OES results, suggesting Ni enrichment on the catalyst surface, an effect that has been observed previously [49]. Therefore, the impregnation of Ni in the second step favors exposes much Ni on the surface.

To understand the oxidation states of the Ni and Cu species, the ratio of Ni^0 or Cu^0 to the total metal content was determined. The monometallic catalysts supported on CC have high Ni^0 or Cu^0 content. The metallic content decreases after the reaction owing to the formation of Ni^{2+}, Cu^{1+}, and Cu^{2+} species, indicating that the metallic particles suffer from the oxidation process. The water generated as a byproduct or solvent (1-butanol) favors the oxidation of the metallic species [37]. In contrast, the catalysts supported on BC has low Ni^0 or Cu^0 content, but the metallic content increases during the reaction, resulting in a reduction of the oxide species. This result can be attributed to the easy reducibility of the oxidized species by the H_2 rich atmosphere, which is favored by the weak interactions between the metallic phases and the support.

The bimetallic catalysts supported on CC have high Ni^0 and Cu^0 species content. After the reaction, Ni is oxidized, whereas Cu is reduced. In contrast, the catalyst supported on BC has low metallic content, which remains almost unchanged after the reaction. In general, much exposure of reduced species on the catalyst surface

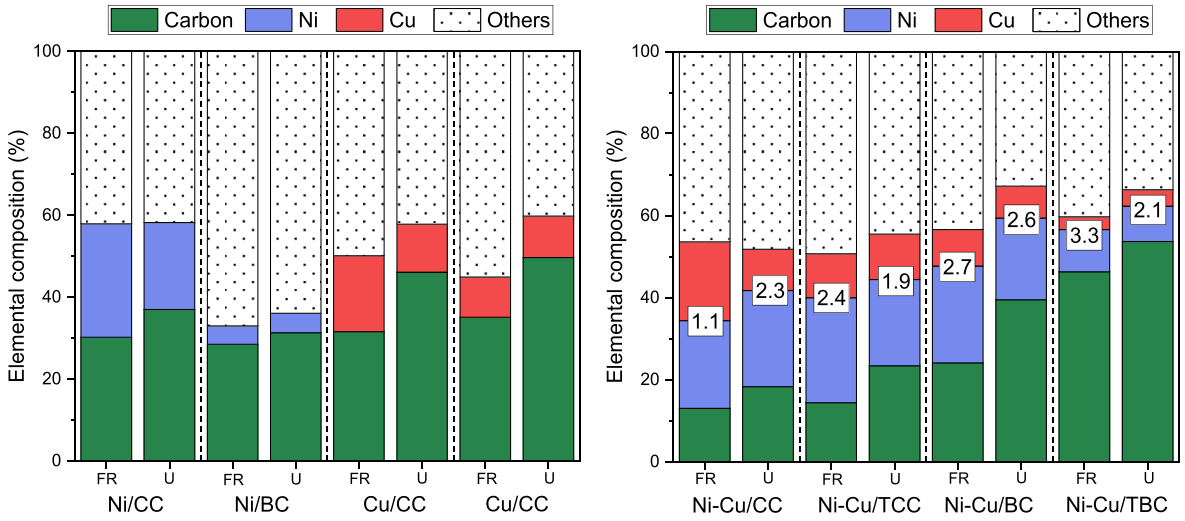

Fig. 4. Elemental composition of different catalysts (others: O, Al, and Si in bimetallic catalysts; the Ni/Cu ratio is expressed in the white box) (operating conditions: T = 275 °C, P_{H_2} = 15 bar, WHSV = 0.15 h^{-1}, and 25 h on stream).

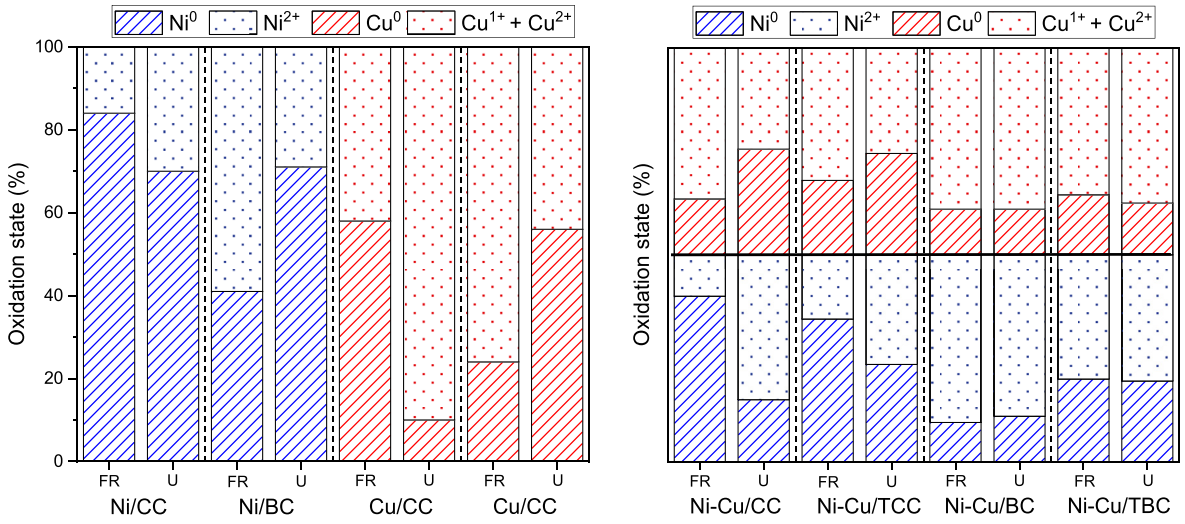

Fig. 5. Oxidation states of Ni and Cu on freshly reduced and used catalysts (operating conditions: T = 275 °C, P_{H_2} = 15 bar, WHSV = 0.15 h^{-1}, and 25 h on stream).

apparently results in the oxidation of some species during the reaction.

It is worth noting that the oxide phases in the XPS spectra are not observed in the XRD patterns, except in the case of the bimetallic catalyst supported on BC. This indicates the high dispersion of oxide species on different catalyst surfaces [53,54].

3.2. Activity results

All the tested catalysts could completely transform the HMF, a platform molecule with high reactivity, under the established operating conditions of 275 °C and 15 bar of H_2 using a space velocity of WHSV = 0.15 h^{-1}. On this basis, the aim is to study and maximize the yields of desired products, namely, DMF and DMTHF, in a time-on-stream manner.

Among all characteristics discussed in previous sections, acidity is the most important in HMF conversion reaction. High acidity can promote C–C cleavage and encourage ring-opening of products [55]; this effect should be avoided because the goal of this study is to optimize the yield of DMF and DMTHF products. However, acidic sites can promote the activation of carbonyl groups and favor the hydrogen transfer reaction [56,57]; they can also play a significant role in anchoring the active metals on the support surface. Therefore, controlled surface acidity is crucial in this process.

3.2.1. Monometallic catalysts

The activities of the monometallic catalysts are summarized in Fig. 6. The monometallic Ni-based catalysts produce DMF and DMTHF in approximately 10 h during the reaction. These products form as a consequence of the reactivity of Ni metallic phases toward C=O and C=C hydrogenation [58]. The Ni/CC catalyst exhibits higher DMTHF yields than DMF yields, probably owing to the presence of much Ni^0 on the surface, which is responsible for C=C bond hydrogenation. However, the DMTHF yield decreases during the reaction, thereby enhancing the DMF yield and producing only DMF at the end of the reaction. After 24 h of reaction, the Ni/CC catalyst apparently loses activity toward DMF formation, resulting in a DMF yield of approximately 45%. The DMF yield of the Ni/BC catalyst is almost constant at approximately 53%. In the case of the Ni/CC catalyst, some Ni^0 species tend to oxidize during the reaction,

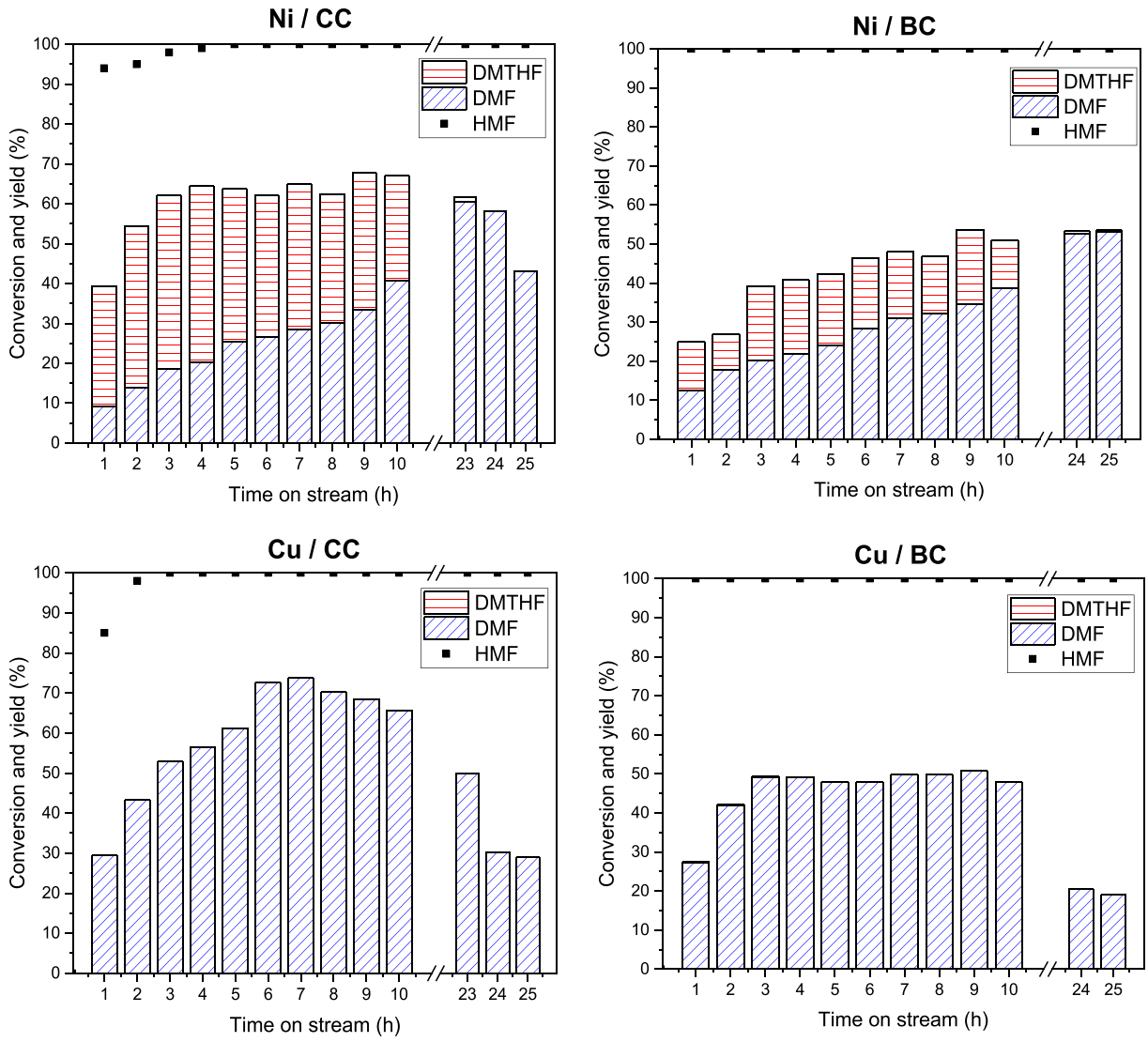

Fig. 6. Conversion and yield for the monometallic catalysts (operating conditions: T = 275 °C, P_{H_2} = 15 bar, and WHSV = 0.15 h^{-1}).

possibly losing their great hydrogenating capacity. However, the Ni/BC catalyst is reduced during the reaction, as corroborated by XPS, resulting in a higher DMF yield than the Ni/CC catalyst.

The Cu-based monometallic catalysts do not produce DMTHF, indicating that their hydrogenation capacity is lower than that of the Ni catalysts because the monometallic Cu catalysts have low metal dispersion and reduced species on the surface. Moreover, Cu has low hydrogenation activity [59]. The obtained DMF yields are approximately 20–30% after 24–25 h of reaction, suggesting a highly pronounced deactivation of these catalysts. The sintering effect (observed in the TEM images; highly profound for Cu/CC) and coke deposition (observed in the XPS spectra) possibly cause the deactivation of these catalysts.

In general, catalysts impregnated on the CC support are more active in yielding the desired products at the beginning of the reaction than those not impregnated. This can be explained by the high metallic content observed on the catalyst surface. Moreover, the low acidity favors the prevention of C–C cleavage and ring-opening product formation, thereby facilitating the production of DMF and DMTHF.

3.2.2. Bimetallic catalysts

The HMF conversion and DMF and DMTHF yields obtained using bimetallic catalysts are outlined in Fig. 7. In general, there is no significant difference between the catalysts supported on untreated (CC and BC) and treated carbons (TCC and TBC). This is advantageous and implies facile synthesis of the catalyst while eliminating the requirement of pretreatment of the support. Moreover, bimetallic catalysts exhibit better stability and higher DMF yields than the corresponding monometallic catalysts, probably because of the interactions between the Ni and Cu metals [37], resulting in a Ni–Cu alloy and a better balance between the acid and metallic sites. Cu can act as a dispersing agent, so it can improve the Ni activity and stability [59].

The catalysts supported on commercial carbon (CC and TCC) exhibit high production rates of the desired DMF and DMTHF during the first 10 h of the reaction, probably because of the high metal content on the catalyst surface and high metallic dispersion, as inferred from XPS and TEM. Moreover, a high DMTHF yield is obtained using these catalysts, which may be related to the metallic Ni^0 on the catalyst surface. Even though the catalysts supported on commercial carbon (CC and TCC) exhibit good catalytic performance at the beginning of the reaction, the results at the end of the

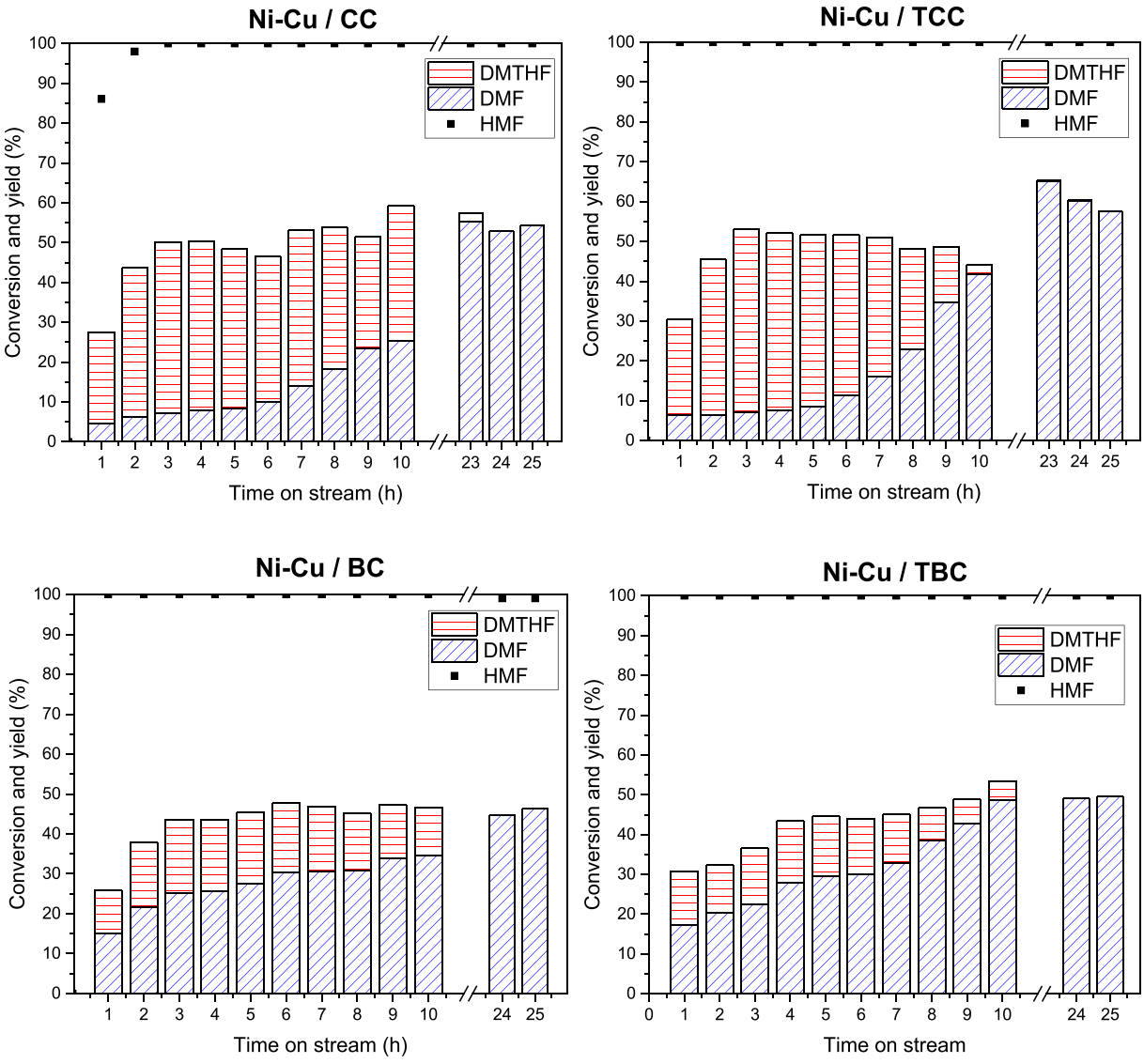

Fig. 7. Conversion and yield for bimetallic catalysts (operating conditions: T = 275 °C, P_{H_2} = 15 bar, and WHSV = 0.15 h^{-1}).

reaction time (25 h) are almost similar for the bimetallic catalysts. Reasonable stability and a DMF yield of approximately 60% for untreated catalysts and 50% for treated ones are achieved. This is in good agreement with the results from the TEM images, in which almost similar particle sizes and dispersions are detected for all the bimetallic catalysts after the reaction and with similar surface acidities measured by NH_3-TPD.

The nonyield of DMTHF by the catalysts supported on commercial carbon (CC and TCC) during the reaction has been reported previously [37]. This effect can be related to the oxidation of Ni^0 during the reaction, by which the furan ring does not get hydrogenated, and DMF is produced. This is in good agreement with the XPS results, where the catalysts supported on CC exhibit Ni oxidation after the reaction.

As reported previously, there is a correlation between the catalytic-test results and catalyst characterization results. The relationship between the DMTHF production at the beginning of the reaction by means of the average yield of DMTHF during the first 3 h of reaction and the metallic Ni content on the freshly reduced catalyst surface, which was calculated from the total Ni amount and Ni^0 ratio, is plotted in Fig. 8. There is a linear and positive correlation between the parameters.

Moreover, the catalysts supported on CC possess high Ni^0 content on the surface, producing much DMTHF at the beginning of the reaction. The high metallic Ni^0 content can result from the metal–support interactions, which enhance the exposure and stability of the metal.

In addition, the metallic Cu on the surface is significant to the total production of DMF and DMTHF during the first stage of the reaction as it can be observed in Fig. 9. Apparently, there is a correlation between the metallic Cu content on the surface and the total mean production of DMF and DMTHF during the first 10 h of the reaction (Fig. 9). The metallic contents of both Cu and Ni are important for the hydrogenolysis of HMF. Cu^0 causes high hydrogenolysis and yields the desired products, whereas Ni^0 enhances the hydrogenation of the C=C bond, resulting in high DMTHF yields.

In general, the measured carbon balances are low because some information regarding the reaction products is misleading. Formation of condensation products is likely; however, the possibility of forming byproducts, such as 5-MF, BHMF, and MFA, was ruled out by the GC–MS analysis, and no peaks of these compounds were

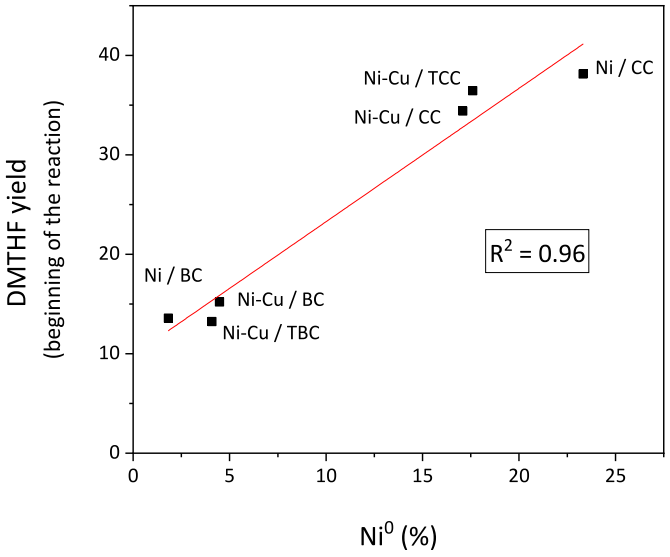

Fig. 8. Relation between metallic Ni content on the catalytic surface and DMTHF yield.

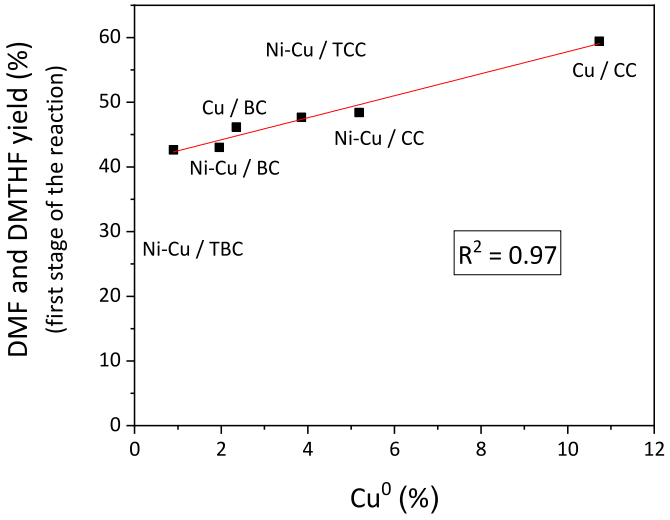

Fig. 9. Relation between metallic Cu content on the catalytic surface and DMF and DMTHF yields.

observed.

Monometallic and bimetallic catalysts have been investigated for the production of DMF via complete HMF conversion. Pomeroy et al. [60] tested activated-carbon-supported Ni, NiLa, and NiNb catalysts at different temperatures and 50 bar of H_2, using THF as the solvent. A DMF selectivity of approximately 75% at 200–230 °C and 3 h of reaction was obtained, slightly higher than that obtained with the catalysts investigated herein. Ru catalysts supported by carbonaceous materials were also tested at lower reaction temperatures (120–150 °C) [61] and 1–10 bar of H_2 pressure. This paper reports a DMF yield close to that obtained by Pomeroy et al. [60] and a DMTHF yield of <5% at 150 °C and 5 bar which correspond to less severe operating conditions) for 1 h. Similar DMF yields were obtained for carbon-supported Ni catalysts at 60 °C and 30 bar [58]; Ni/SiO_2 and Raney Ni catalysts were highly selective toward DMTHF formation. Esteves et al. [14] performed HMF hydrogenation over supported Cu catalysts at 200 °C and 20 bar of H_2 and achieved a DMF yield of approximately 90% for Al_2O_3- and modified-Al_2O_3-supported Cu catalysts. These catalysts provided moderate total acidity and high metal dispersion, which is presumed crucial for DMF formation via the activation of the oxygen of the hydroxyl groups on HMF. Low DMF yield of 75% was obtained by employing a Cu/Al_2O_3 catalyst at 240 °C and 7 mL methanol as the hydrogen donor [62].

Regarding bimetallic catalysts, the literature has reported the use of hydrotalcite- and SBA-16 supported NiCu catalysts [26,63]. The NiCu/HT catalyst could completely convert HMF into DMF (67%) and DMTHF (32%) at 90 °C and 10 bar of H_2 after 15 h of reaction [26]. The 5Ni12Cu/SBA-16 catalyst provided a DMF yield of approximately 63% under severe operating conditions (210 °C and 20 bar after 4 h) [63]. Other bimetallic-catalyst activities have also been reported in the literature. Wang et al. [15] obtained 90% DMF yield at 10 bar of H_2 and 160 °C using a noble-metal-based Pt–Co bimetallic catalyst. Similar results were obtained by Chen et al. [24], who used a non-noble-metal-based Cu–Co@C catalyst, which resulted in 99 %DMF yield.

In conclusion, the activity and selectivity data presented herein are in the range of those reported in the literature, the difference that the reported studies used batch reactors and liquid-phase reactions to test catalytic systems. The DMF and DMTHF selectivities or yields strongly depend on the type of reactor used in the measurements [64], operating conditions, and choice of catalysts. Evidently, comparable yields can be achieved using a continuous fixed-bed reactor, thereby inching closer to industrial application prospects. Moreover, the use of carbonaceous supports produced from local biomass residues leads to highly sustainable catalyst development.

3.2.3. Catalyst stability and reusability

Stability and reusability experiment was performed with the most promising catalyst, Ni–Cu/BC. In Fig. 10 it can be observed that this catalyst was stable for 46 h on stream and continued producing the desired product, exhibiting a DMF yield of 40% after 53 h on stream. However, the catalyst was gradually deactivated, presumably caused by poisoning by carbon deposition or as a result of metal sintering. In order to reactivate the catalyst, pure hydrogen was in-situ flowed edit the reactor during the night at the reaction temperature (275 C). After the reactivation at the reaction temperature, DMF yield did not exceed 20% and formation of 5-MF was

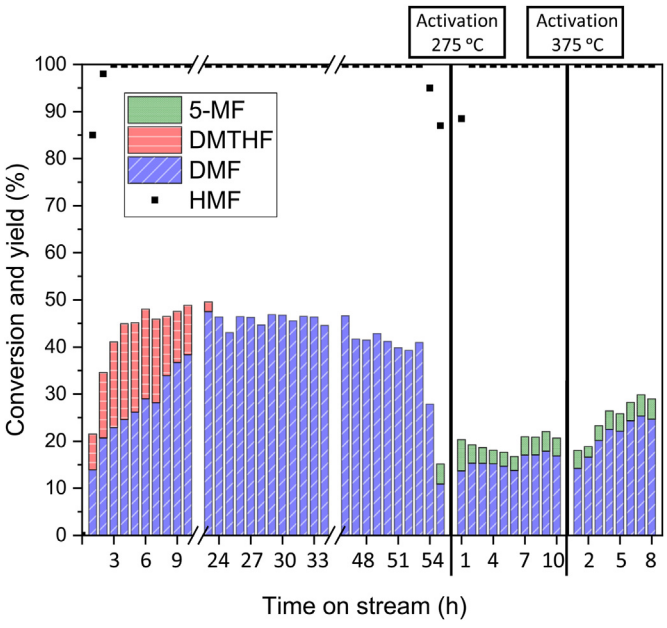

Fig. 10. Stability and reusability of Ni–Cu/BC.

detected. These results suggest that the catalyst has lost its hydrogenation capacity. Consequently, the catalyst was reactivated following the previous procedure during the night at 375 C. It seems that the thermal treatments slightly improved the hydrogenation capacity of the catalyst, reaching 25% of DMF. However, these results are not close to the optimum obtained after 24 h on stream.

4. Conclusions

Hydrogenolysis of HMF to produce DMF and DMTHF was studied in a continuous fixed-bed reactor using Ni- and/or Cu-based catalysts supported on CC and BC. Kaolin was incorporated into the support to enhance the mechanical properties of the bare carbons. Monometallic and bimetallic catalysts were synthesized to understand the effect of each metal. The carbon supports were treated with HNO_3 and subsequently neutralized with NaOH to remove any carbonaceous impurities. These treated carbons were only employed to prepare bimetallic catalysts.

The bimetallic catalysts, regardless of the support, exhibits an excellent balance of acid sites and metallic sites (NiCu active species) to achieve stable operation. It has been previously reported that NiCu has lower activation energies than pure Ni, and consequently, lower reaction barriers [31]. Slightly higher than 50% DMF yield was achieved after 25 h on stream in all the bimetallic catalysts. For further stability tests, coke deposition in all catalysts should be taken account off. Moreover, Ni–Cu/BC catalyst exhibited a promising stability, reaching 45% of DMF yield after 46 h on stream.

Monometallic Ni catalysts produced DMTHF; however, the Cu-based catalysts could not produce DMTHF. This stresses the need for a reduced Ni species to hydrogenate the C=C bond. In general, monometallic catalysts show high yields of the desired products at the beginning of the reaction. However, the catalysts, except for Ni/BC, were deactivated, probably because of the sintering of the metallic active sites. This effect is very severe in the case of Cu-based catalysts.

CC has higher Ni and/or Cu surface content and Ni^o and/or Cu^o surface content than BC. This leads to a higher yield of desired products by CC than by BC at the beginning of the reaction. However, similar results were obtained for both supports after 25 h of reaction.

Finally, the metallic content of Cu strongly influences the total production of DMF and DMTHF during the initial few hours of the reaction. Similarly, metallic Ni is correlated with the hydrogenation capacity of the C=C bond of the catalyst.

The use of biomass-derived carbon as a catalyst support results in high DMF and DMTHF yields. Therefore, the application of this material to catalytic processes will increase the sustainability of the processes.

Funding sources

This study was supported by the University of the Basque Country (EHU/UPV), the University of Malaga (UMA) [Grant number: UMA18-FEDERJA-171], the Spanish Ministry of Economy and Innovation, the European Union through the European Regional Development Fund (ERDF) [Grant number: RTI2018-094918-B-C43 and RTI2018-94918-B-C44], and the Basque Government [Grant number: IT993-16].

Credit author statement

Fuel Processing Technology, All authors have participated in the research and each author has contributed to the article as follows: **Nerea Viar**: conceptualization, formal analysis, investigation, methodology, visualization, writing – original draft, writing – review & editing.; **Jesús M. Requies**: conceptualization, funding acquisition, investigation, methodology, project administration, resources, supervision, writing – review & editing.; **Ion Agirre**: conceptualization, funding acquisition, investigation, methodology, project administration, resources, supervision, writing – review & editing.; **Aitziber Iriondo**: conceptualization, funding acquisition, investigation, project administration, resources, supervision, writing – review & editing.; **Cristina García-Sancho**: conceptualization, funding acquisition, investigation, project administration, resources, supervision, writing – review & editing; **Pedro L. Arias**: conceptualization, funding acquisition, investigation, project administration, resources, supervision, writing – review & editing.; All authors agree with the contents and to the submission.

Declaration of competing interest

The authors declare that they have no known competing financial interests or personal relationships that could have appeared to influence the work reported in this paper.

Acknowledgments

The authors thank for technical and human support provided by SGiker (UPV/EHU/ERDF, EU), Envirohemp S.L. for providing biomass-derived carbon, and Pedro J. Maireles (University of Malaga) for his assistance with the XPS results and the SEM analysis.

Appendix A. Supplementary data

Supplementary data to this article can be found online at https://doi.org/10.1016/j.energy.2022.124437.

References

[1] International Energy Agency (IEA). World energy outlook 2019. Executive Summary. TemaNord 2019:7–15. https://doi.org/10.6027/9789289329996-1-en.
[2] Change in final energy consumption by sector, 2000-2018, and by scenario to 2040 – Charts – Data & Statistics - IEA n.d. https://www.iea.org/data-and-statistics/charts/change-in-final-energy-consumption-by-sector-2000-2018-and-by-scenario-to-2040. [Accessed 11 May 2020]. accessed.
[3] International Energy Agency. World energy balances: an Overview. J Chem Inf Model 2019;53:1689–99. https://doi.org/10.1017/CBO9781107415324.004.
[4] Jing Y, Guo Y, Xia Q, Liu X, Wang Y. Catalytic production of value-added chemicals and liquid fuels from lignocellulosic biomass. Inside Chem 2019;5:2520–46. https://doi.org/10.1016/j.chempr.2019.05.022.
[5] Bozell JJ, Petersen GR. Technology development for the production of biobased products from biorefinery carbohydrates - the US Department of Energy's "top 10" revisited. Green Chem 2010;12:539–54. https://doi.org/10.1039/b922014c.
[6] Xia H, Xu S, Hu H, An J, Li C. Efficient conversion of 5-hydroxymethylfurfural to high-value chemicals by chemo- and bio-catalysis. RSC Adv 2018;8:30875–86. https://doi.org/10.1039/C8RA05308A.
[7] Viar N, Requies JM, Agirre I, Iriondo A, Arias PL. Furanic biofuels production from biomass using Cu-based heterogeneous catalysts. Energy 2019;172:531–44. https://doi.org/10.1016/j.energy.2019.01.109.
[8] Tzeng TW, Lin CY, Pao CW, Chen JL, Nuguid RJG, Chung PW. Understanding catalytic hydrogenolysis of 5-hydroxymethylfurfural (HMF) to 2,5-dimethylfuran (DMF) using carbon supported Ru catalysts. Fuel Process Technol 2020;199:106225. https://doi.org/10.1016/j.fuproc.2019.106225.
[9] Raut AB, Nanda B, Parida KM, Bhanage BM. Hydrogenolysis of biomass-derived 5-hydroxymethylfurfural to produce 2,5-dimethylfuran over Ru-ZrO2-MCM-41 catalyst. ChemistrySelect 2019;4:6080–9. https://doi.org/10.1002/slct.201901145.
[10] Shi J, Wang Y, Yu X, Du W, Hou Z. Production of 2,5-dimethylfuran from 5-hydroxymethylfurfural over reduced graphene oxides supported Pt catalyst under mild conditions. Fuel 2016;163:74–9. https://doi.org/10.1016/j.fuel.2015.09.047.
[11] Guo D, Liu X, Cheng F, Zhao W, Wen S, Xiang Y, et al. Selective hydrogenolysis of 5-hydroxymethylfurfural to produce biofuel 2, 5-dimethylfuran over Ni/ZSM-5 catalysts. Fuel 2020;274:117853. https://doi.org/10.1016/j.fuel.2020.117853.

[12] Sarkar C, Paul R, Chandra Shit S, Trinh QT, Koley P, Rao BS, et al. Navigating copper-atom-pair structural effect inside a porous organic polymer cavity for selective hydrogenation of biomass-derived 5-hydroxymethylfurfural. ACS Sustainable Chem Eng 2021;9:2136–51. https://doi.org/10.1021/acssuschemeng.0c07594.
[13] Zhang Z, Wang C, Gou X, Chen H, Chen K, Lu X, et al. Catalytic in-situ hydrogenation of 5-hydroxymethylfurfural to 2,5-dimethylfuran over Cu-based catalysts with methanol as a hydrogen donor. Appl Catal Gen 2019;570:245–50. https://doi.org/10.1016/j.apcata.2018.11.029.
[14] Esteves LM, Brijaldo MH, Oliveira EG, Martinez JJ, Rojas H, Caytuero A, et al. Effect of support on selective 5-hydroxymethylfurfural hydrogenation towards 2,5-dimethylfuran over copper catalysts. Fuel 2020;270:117524. https://doi.org/10.1016/j.fuel.2020.117524.
[15] Wang X, Liu Y, Liang X. Hydrogenolysis of 5-hydroxymethylfurfural to 2,5-dimethylfuran over supported Pt-Co bimetallic catalysts under mild conditions. Green Chem 2018;20:2894–902. https://doi.org/10.1039/c8gc00716k.
[16] Liao W, Zhu Z, Chen N, Su T, Deng C, Zhao Y, et al. Highly active bifunctional Pd-Co9S8/S-CNT catalysts for selective hydrogenolysis of 5-hydroxymethylfurfural to 2,5-dimethylfuran. Mol Catal 2020;482:110756. https://doi.org/10.1016/j.mcat.2019.110756.
[17] Chen N, Zhu Z, Su T, Liao W, Deng C, Ren W, et al. Catalytic hydrogenolysis of hydroxymethylfurfural to highly selective 2,5-dimethylfuran over FeCoNi/h-BN catalyst. Chem Eng J 2020;381:122755. https://doi.org/10.1016/j.cej.2019.122755.
[18] Han W, Tang M, Li J, Li X, Wang J, Zhou L, et al. Selective hydrogenolysis of 5-hydroxymethylfurfural to 2,5-dimethylfuran catalyzed by ordered mesoporous alumina supported nickel-molybdenum sulfide catalysts. Appl Catal B Environ 2020;268:118748. https://doi.org/10.1016/j.apcatb.2020.118748.
[19] Luo J, Lee JD, Yun H, Wang C, Monai M, Murray CB, et al. Base metal-Pt alloys: a general route to high selectivity and stability in the production of biofuels from HMF. Appl Catal B Environ 2016;199:439–46. https://doi.org/10.1016/j.apcatb.2016.06.051.
[20] De S, Zhang J, Luque R, Yan N. Ni-based bimetallic heterogeneous catalysts for energy and environmental applications. Energy Environ Sci 2016;9:3314–47. https://doi.org/10.1039/c6ee02002j.
[21] Yang P, Xia Q, Liu X, Wang Y. High-yield production of 2,5-dimethylfuran from 5-hydroxymethylfurfural over carbon supported Ni–Co bimetallic catalyst. J Energy Chem 2016;25:1015–20. https://doi.org/10.1016/j.jechem.2016.08.008.
[22] Guo W, Liu H, Zhang S, Han H, Liu H, Jiang T, et al. Efficient hydrogenolysis of 5-hydroxymethylfurfural to 2,5-dimethylfuran over a cobalt and copper bimetallic catalyst on N-graphene-modified Al2O3. Green Chem 2016;18:6222–8. https://doi.org/10.1039/c6gc02630c.
[23] Srivastava S, Jadeja GC, Parikh J. Influence of supports for selective production of 2,5-dimethylfuran via bimetallic copper-cobalt catalyzed 5-hydroxymethylfurfural hydrogenolysis. Cuihua Xuebao/Chin J Catal 2017;38:699–709. https://doi.org/10.1016/S1872-2067(17)62789-X.
[24] Chen B, Li F, Huang Z, Yuan G. Carbon-coated Cu-Co bimetallic nanoparticles as selective and recyclable catalysts for production of biofuel 2 , 5-dimethylfuran. Appl Catal B Environ 2017;200:192–9. https://doi.org/10.1016/j.apcatb.2016.07.004.
[25] Sarkar C, Koley P, Shown I, Lee J, Liao YF, An K, et al. Integration of interfacial and alloy effects to modulate catalytic performance of metal-organic-framework-derived Cu-Pd nanocrystals toward hydrogenolysis of 5-hydroxymethylfurfural. ACS Sustainable Chem Eng 2019;7:10349–62. https://doi.org/10.1021/acssuschemeng.9b00350.
[26] Gupta D, Kumar R, Pant KK. Hydrotalcite supported bimetallic (Ni-Cu) catalyst: a smart choice for one-pot conversion of biomass-derived platform chemicals to hydrogenated biofuels. Fuel 2020;277:118111. https://doi.org/10.1016/j.fuel.2020.118111.
[27] Gao Z, Li C, Fan G, Yang L, Li F. Nitrogen-doped carbon-decorated copper catalyst for highly efficient transfer hydrogenolysis of 5-hydroxymethylfurfural to convertibly produce 2,5-dimethylfuran or 2,5-dimethyltetrahydrofuran. Appl Catal B Environ 2018;226:523–33. https://doi.org/10.1016/j.apcatb.2018.01.006.
[28] Chen S, Ciotonea C, De Oliveira Vigier K, Jérôme F, Wojcieszak R, Dumeignil F, et al. Hydroconversion of 5-hydroxymethylfurfural to 2,5-dimethylfuran and 2,5-dimethyltetrahydrofuran over non-promoted Ni/SBA-15. ChemCatChem 2020;12. https://doi.org/10.1002/cctc.201902028. 2050–9.
[29] Hu Q, Jung J, Chen D, Leong K, Song S, Li F, et al. Biochar industry to circular economy. Sci Total Environ 2021;757:143820. https://doi.org/10.1016/j.scitotenv.2020.143820.
[30] Kempasiddaiah M, Sree Raj KA, Kandathil V, Dateer RB, Sasidhar BS, Yelamaggad CV, et al. Waste biomass-derived carbon-supported palladium-based catalyst for cross-coupling reactions and energy storage applications. Appl Surf Sci 2021;570:151156. https://doi.org/10.1016/j.apsusc.2021.151156.
[31] Wang Y, Furukawa S, Yan N. Identification of an active NiCu catalyst for nitrile synthesis from alcohol. ACS Catal 2019;9:6681–91. https://doi.org/10.1021/acscatal.9b00043.
[32] Safarov J, Ahmadov B, Mirzayev S, Shahverdiyev A, Hassel E. Vapor pressures of 1-butanol over wide range of temperatures. Chemistry 2015;24:226–46.
[33] Du X, Kong X, Chen L. Influence of binder on catalytic performance of Ni/HZSM-5 for hydrodeoxygenation of cyclohexanone. Catal Commun 2014;45:109–13. https://doi.org/10.1016/j.catcom.2013.10.042.
[34] Hussein A, Larachi F, Ziegler D, Alamdari H. Effects of heat treatment and acid washing on properties and reactivity of charcoal. Biomass Bioenergy 2016;90:101–13. https://doi.org/10.1016/j.biombioe.2016.03.041.
[35] Zhao Z, Lu W, Zhu H, Dong W, Lyu Y, Liu T, et al. Tuning the fischer–tropsch reaction over CoxMnyLa/AC catalysts toward alcohols: effects of La promotion. J Catal 2018;361:156–67. https://doi.org/10.1016/j.jcat.2018.02.008.
[36] Zhao Z, Lu W, Feng C, Chen X, Zhu H, Yang R, et al. Increasing the activity and selectivity of Co-based FTS catalysts supported by carbon materials for direct synthesis of clean fuels by the addition of chromium. J Catal 2019;370:251–64. https://doi.org/10.1016/j.jcat.2018.12.022.
[37] Viar N, Requies JM, Agirre I, Iriondo A, Gil-Calvo M, Arias PL. Ni-Cu bimetallic catalytic system for producing 5-hydroxymethylfurfural-derived value-added biofuels. ACS Sustainable Chem Eng 2020;8:11183–93. https://doi.org/10.1021/acssuschemeng.0c02433.
[38] Borodziński A, Bonarowska M. Relation between crystallite size and dispersion on supported metal catalysts. Langmuir 1997;13:5613–20. https://doi.org/10.1021/la962103u.
[39] Cao Y, Sio Z, Zhu Y, Zhou X, Chen D. Selective hydrogenation of acetylene over Pd-In/Al2O3 catalyst: promotional effect of indium and composition-dependent performance. ACS Catal 2017;7:7835–46. https://doi.org/10.1021/acscatal.7b01745.
[40] Matos I, Neves PD, Castanheiro JE, Perez-Mayoral E, Martin-Aranda R, Duran-Valle C, et al. Mesoporous carbon as an efficient catalyst for alcoholysis and aminolysis of epoxides. Appl Catal Gen 2012;439–440:24–30. https://doi.org/10.1016/j.apcata.2012.06.036.
[41] Brazil TR, Junior MSO, Baldan MR, Massi M, Rezende MC. Effect of different superficial treatments on structural, morphological and superficial area of Kraft lignin based charcoal. Vib Spectrosc 2018;99:130–6. https://doi.org/10.1016/j.vibspec.2018.08.021.
[42] Pastor-Pérez L, Gu S, Sepúlveda-Escribano A, Reina TR. Bimetallic Cu–Ni catalysts for the WGS reaction – cooperative or uncooperative effect? Int J Hydrogen Energy 2019;44:4011–9. https://doi.org/10.1016/j.ijhydene.2018.12.127.
[43] de Andrade TS, Souza MMVM, Manfro RL. Hydrogenolysis of glycerol to 1,2-propanediol without external H2 addition in alkaline medium using Ni-Cu catalysts supported on Y zeolite. Renew Energy 2020;160:919–30. https://doi.org/10.1016/j.renene.2020.06.060.
[44] Li FX, Wang XF, Zheng Y, Chen JX. Influence of metallic promoters on the performance of Ni/SiO2 catalyst in the hydrodeoxygenation of anisole. Ranliao Huaxue Xuebao/J Fuel Chem Technol 2018;46:75–83. https://doi.org/10.1016/s1872-5813(18)30005-7.
[45] Wang X, Chen J. Effects of indium on Ni/SiO2 catalytic performance in hydrodeoxygenation of anisole as model bio-oil compound: suppression of benzene ring hydrogenation and C-C bond hydrogenolysis. Cuihua Xuebao/Chin J Catal 2017;38:1818–30. https://doi.org/10.1016/S1872-2067(17)62910-3.
[46] Yang Z, Liu Y, Liu D, Meng X, Liu C. Hydroisomerization of n-octane over bimetallic Ni-Cu/SAPO-11 catalysts. Appl Catal Gen 2017;543:274–82. https://doi.org/10.1016/j.apcata.2017.06.028.
[47] Li X, Xiang M, Wu D. Hydrogenolysis of glycerol over bimetallic Cu–Ni catalysts supported on hierarchically porous SAPO-11 zeolite. Catal Commun 2019;119:170–5. https://doi.org/10.1016/j.catcom.2018.11.004.
[48] Guo X, Zhu L, Li W, Yang H. Preparation of SiC powders by carbothermal reduction with bamboo charcoal as renewable carbon source. J Adv Ceram 2013;2:128–34. https://doi.org/10.1007/s40145-013-0050-4.
[49] Liu H, Huang Z, Kang H, Li X, Xia C, Chen J, et al. Efficient bimetallic NiCu-SiO2 catalysts for selective hydrogenolysis of xylitol to ethylene glycol and propylene glycol. Appl Catal B Environ 2018;220:251–63. https://doi.org/10.1016/j.apcatb.2017.08.022.
[50] Zhu J, Chen F, Zhang Z, Li M, Yang Q, Yang Y, et al. M-gallate (M = Ni, Co) metal-organic framework-derived Ni/C and bimetallic Ni-Co/C catalysts for lignin conversion into monophenols. ACS Sustainable Chem Eng 2019;7:12955–63. https://doi.org/10.1021/acssuschemeng.9b02005.
[51] Requies J, Güemez MB, Maireles P, Iriondo A, Barrio VL, Cambra JF, et al. Zirconia supported Cu systems as catalysts for n-butanol conversion to butyraldehyde. Appl Catal Gen 2012;423–424:185–91. https://doi.org/10.1016/j.apcata.2012.02.039.
[52] Gupta D, Kumar R, Pant KK. Hydrotalcite supported bimetallic (Ni-Cu) catalyst: a smart choice for one-pot conversion of biomass-derived platform chemicals to hydrogenated biofuels. Fuel 2020;277:118111. https://doi.org/10.1016/j.fuel.2020.118111.
[53] Freitas IC, Manfro RL, Souza MMVM. Hydrogenolysis of glycerol to propylene glycol in continuous system without hydrogen addition over Cu-Ni catalysts. Appl Catal B Environ 2018;220:31–41. https://doi.org/10.1016/j.apcatb.2017.08.030.
[54] Cai F, Pan D, Ibrahim JJ, Zhang J, Xiao G. Hydrogenolysis of glycerol over supported bimetallic Ni/Cu catalysts with and without external hydrogen addition in a fixed-bed flow reactor. Appl Catal Gen 2018;564:172–82. https://doi.org/10.1016/j.apcata.2018.07.029.
[55] Zhou CH, Deng K, Serio M Di, Xiao S, Tong DS, Li L, et al. Cleaner hydrothermal hydrogenolysis of glycerol to 1,2-propanediol over Cu/oxide catalysts without addition of external hydrogen. Mol Catal 2017;432:274–84. https://doi.org/10.1016/j.mcat.2017.02.008.
[56] Zhang J, Chen T, Jiao Y, Wang L, Wang J, Chen Y, et al. Role of acidity in catalytic cracking of n-decane over supported Pt-based catalysts. Appl Surf Sci

2020;507:145113. https://doi.org/10.1016/j.apsusc.2019.145113.
[57] Zhu Y, Kong X, Zheng H, Ding G, Zhu Y, Li YW. Efficient synthesis of 2,5-dihydroxymethylfuran and 2,5-dimethylfuran from 5-hydroxymethylfurfural using mineral-derived Cu catalysts as versatile catalysts. Catal Sci Technol 2015;5:4208–17. https://doi.org/10.1039/c5cy00700c.
[58] Morales MV, Conesa JM, Guerrero-Ruiz A, Rodríguez-Ramos I. Tunable selectivity of Ni catalysts in the hydrogenation reaction of 5-hydroxymethylfurfural in aqueous media: role of the carbon supports. Carbon N Y 2021;182:265–75. https://doi.org/10.1016/j.carbon.2021.06.007.
[59] Deng L, Ai X, Xie F, Zhou G. Efficient Ni-based catalysts for low-temperature reverse water-gas shift (RWGS) reaction. Chem Asian J 2021;16:949–58. https://doi.org/10.1002/asia.202100100.
[60] Pomeroy B, Grilc M, Gyergyek S, Likozar B. Catalyst structure-based hydroxymethylfurfural (HMF) hydrogenation mechanisms, activity and selectivity over Ni. Chem Eng J 2021:412. https://doi.org/10.1016/j.cej.2020.127553.
[61] Tzeng TW, Lin CY, Pao CW, Chen JL, Nuguid RJG, Chung PW. Understanding catalytic hydrogenolysis of 5-hydroxymethylfurfural (HMF) to 2,5-dimethylfuran (DMF) using carbon supported Ru catalysts. Fuel Process Technol 2020;199:106225. https://doi.org/10.1016/j.fuproc.2019.106225.
[62] Zhang Z, Wang C, Gou X, Chen H, Chen K, Lu X, et al. Catalytic in-situ hydrogenation of 5-hydroxymethylfurfural to 2,5-dimethylfuran over Cu-based catalysts with methanol as a hydrogen donor. Appl Catal Gen 2019;570:245–50. https://doi.org/10.1016/j.apcata.2018.11.029.
[63] Umasankar S, Tamizhdurai P, Santhana krishnan P, Narayanan S, Mangesh VL, Shanthi K. Effect of copper on NiCu bimetallic catalyst supported on SBA-16 for the catalytic hydrogenation of 5-hydroxymethylfurfural to 2,5-dimethylfuran. Biomass Bioenergy 2020;143:105868. https://doi.org/10.1016/j.biombioe.2020.105868.
[64] Luo J, Arroyo-Ramírez L, Wei J, Yun H, Murray CB, Gorte RJ. Comparison of HMF hydrodeoxygenation over different metal catalysts in a continuous flow reactor. Appl Catal Gen 2015;508:86–93. https://doi.org/10.1016/j.apcata.2015.10.009.